Available online at www.sciencedirect.com
SCIENCE DIRECT®
Journal of Magnetic Resonance 176 (2005) 171–178
JMR Journal of Magnetic Resonance
www.elsevier.com/locate/jmr

Improvement of duty-cycle heating compensation in NMR spin relaxation experiments

Grover N.B. Yip [a], Erik R.P. Zuiderweg [a,b,c,*]

[a] Department of Chemistry, University of Michigan, 930 N. University Ave., MI 48109-1055, USA
[b] Department of Biological Chemistry, University of Michigan, 930 N. University Ave., MI 48109-1055, USA
[c] Biophysics Research Division, University of Michigan, 930 N. University Ave., MI 48109-1055, USA

Received 8 March 2005; revised 27 May 2005
Available online 11 July 2005

Abstract

To reliably measure NMR relaxation properties of macromolecules is a prerequisite for precise experiments that identify subtle variations in relaxation rates, as required for the determination of rotational diffusion anisotropy, CSA tensor determination, advanced motional modeling or entropy difference estimations. An underlying problem with current NMR relaxation measurement protocols is maintaining constant sample temperature throughout the execution of the relaxation series especially when rapid data acquisition is required. Here, it is proposed to use a combination of a heating compensation and a proton saturation sequence at the beginning of the NMR relaxation pulse scheme. This simple extension allows reproducible, robust and rapid acquisition of NMR spin relaxation data sets. The method is verified with ^{15}N spin relaxation measurements for human ubiquitin.

Keywords: CPMG; Transverse (T_2) relaxation; Longitudinal (T_1) relaxation; Duty cycle; Radiofrequency irradiation; Sample heating

1. Introduction

The study of dynamics by NMR affords invaluable insight in biomolecular function [1–8]. A handful of spin relaxation experiments (e.g., longitudinal (T_1), transverse (T_2), $T_{1\rho}$, NOE) are in the ideal case capable of measuring precise relaxation properties that describe the pico to nano second dynamics [9–12] and micro to milli second dynamics [13] of the internuclear vectors of interest. In addition, relaxation experiments are used to determine rotational diffusion anisotropy [14,15], CSA tensors [16–18], and are essential to advanced motional modeling [19–22] or entropy estimations [23–25]. A necessary part of any spin relaxation pulse sequence is the relaxation time (RT),[1] which is varied per spectrum in the (2D) relaxation series (RS), see Fig. 1. Accordingly, the duty cycle of the radiofrequency (RF) irradiation of the sample by the pulse sequence varies between the different spectra in the RS. This duty cycle variation occurs in principle in all spin relaxation experiments, but the effect is largest in experiments in which the RT contains CPMG with short interpulse delays or spinlock RF trains. A direct consequence is that the NMR sample temperature varies between the spectra in the RS, despite instrumental means to control temperature. Change in sample temperature results in

* Corresponding author. Fax: +1 734 764 3323.
E-mail address: zuiderwe@umich.edu (E.R.P. Zuiderweg).

[1] *Abbreviations:* RT, relaxation time; DCC, duty cycle compensation; PSS, pre-scan saturation; RF, radiofrequency; v_1, traditional pulse scheme; v_2, modified pulse scheme with DCC and PSS; RS, relaxation series; CPMG, Carr–Purcell–Meiboom–Gill; t_{RcvyD}, total recovery delay; PFG, pulsed-field gradient.

1090-7807/$ - see front matter
doi:10.1016/j.jmr.2005.06.003

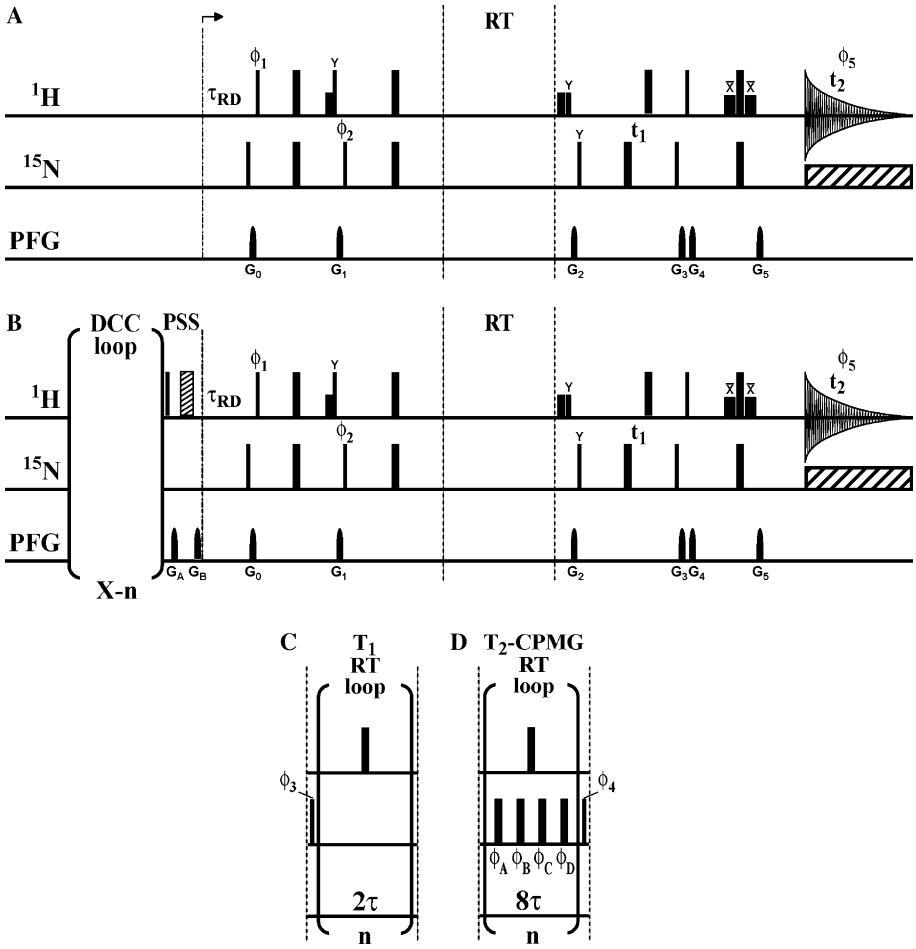

Fig. 1. (A) Generic representation of a conventional 2D-HSQC detected ^{15}N relaxation pulse sequence, denoted as v_1 pulse scheme. (B) Generic representation of the modified relaxation experiment in which duty cycle compensation (DCC) and pre-scan saturation (PSS) blocks are included, denoted as the v_2 pulse scheme. The blank relaxation mixing time (RT) block in A or B can be filled with either: (C) a T_1 loop with sparse ^{1}H pulses for cross-correlation suppression or (D) T_2-CPMG with cross-correlation suppression. The DCC loop consists of an *exact* copy the RT loop scheme, including powers, offsets and pulse shapes, corresponding to the type of relaxation experiment in use. τ_{RD}, recovery delay. The water resonance was kept saturated in both sequences by the use of a 1 ms X-phase spin lock purge pulse in the ^{1}H–^{15}N INEPT, and a 1 ms and 500 μs cross-phase ^{1}H crusher pulses after the RT block. Solvent suppression during data acquisition was achieved by a Watergate scheme. Sensitivity enhancement of the HSQC can be used for very small molecule applications, while a sensitivity-enhanced TROSY detection scheme can be used for large molecules. All experiments were acquired with a 245.8 ms acquisition time with (128×4096) total complex points and spectral widths of (3333.33×8333.33) Hz at (117.846×4.707) ppm carrier positions in the (t_1-^{15}N × t_2-^{1}H) dimensions, respectively, for an average run time of 20–50 min per 2D spectrum. T_1 loops ran with $\tau = 5$ ms and a 20 μs ^{1}H π pulse (full power). T_2-CPMG loops ran with $\tau = 350$ μs ($\tau_{CPMG} = 700$ μs), a 40-μs ^{1}H π pulse, and 200 μs ^{15}N π pulses. All pulses are $+X$ phase unless otherwise indicated; bars over the X or Y signify negative phases. For T_1 experiments the following phase cycling was used: $\phi_1[X]$, $\phi_2[X,-X]$, $\phi_3[Y,Y,-Y,-Y]$, and $\phi_5[X,-X,-X,X]$. For T_2-CPMG experiments the following phase cycling was used $\phi_1[X,X,-X-X]$, $\phi_2[X,-X]$, $\phi_4[Y,Y,Y,Y,-Y,-Y,-Y,-Y]$, and $\phi_5[X,-X,-X,X,-X,X,X,-X]$. A T_2-CPMG RT loop phase cycling of $[\phi_A,\phi_B,\phi_C,\phi_D] = [X,X,Y,-Y]$ was employed to improve the uniformity of the sequence over the ^{15}N spectral width [36]. The following 1ms half-sine shaped pulsed-field gradients (PFG, in G/cm) were applied $G_0 = -48y$, $G_1 = G_4 = G_5 = 24z$, $G_2 = -45x$, and $G_3 = 39y$. Each relaxation series (RS) consisted of RT loop number settings: 1, 17, and 74 (10, 170, and 740 ms, respectively) for T_1; and 1, 12, and 35 (2.8, 33.6, and 98 ms, respectively) for T_2-CPMG. The RS were carried out in triplicate for purposes of analyzing the data statistics. The PSS sequence consisted of a non-selective ^{1}H π/2 pulse along x, followed by a 1 ms half-sine shaped Z-PFG of 12 G/cm peak amplitude (G_A), followed by a 1 ms full power spin lock along x, followed by a 1 ms half-sine shaped X-PFG of 48 G/cm peak amplitude (G_B). All ^{15}N decoupling during t_2 acquisition was achieved with 3.3 kHz WALTZ-16 [37] for the duration of t_2 (~246 ms).

a shift of the ^{2}H resonance of the ^2H_2O (−0.01145 ppm/deg) to which the instrument is locked, leading to an apparent (and opposite) change in resonance frequencies of the solute. For example, the NH cross-peaks in panels A and C of Fig. 2, which are part of a ^{15}N T_1 relaxation series, appear to be shifting in the set of overlaid spectra for which the only change is a change in RT. Sometimes these problems can be corrected at data-analysis time by recalibrating the spectra; but in severe cases the shifts can be non-uniform, making data analysis less robust. In addition, the dynamic processes underlying T_1 and T_2 and especially conformational exchange rates are intrinsically temperature dependent, which in some cases may lead to errors in the RS that cannot be corrected

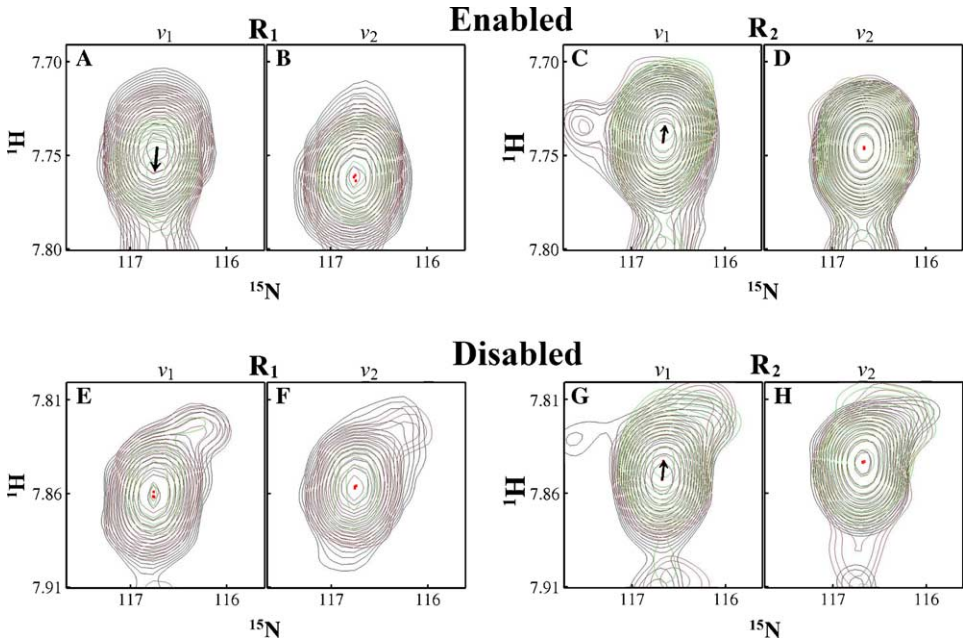

Fig. 2. Each panel is an overlay contour plot of three spectra from a relaxation series (RS) for the ^{1}H–^{15}N cross-peak of residue 40 of human ubiquitin. The panels compare the results of v_1 and v_2 style pulse sequences for T_1 and T_2-CPMG with or without ^{15}N acquisition decoupling as indicated. Each overlay consisted spectra with 10, 170, and 740 ms RT for T_1; and 2.8, 33.6, and 98 ms RT for T_2-CPMG. Red dots illustrate the peak centers for the different spectra contours of varying relaxation times (RT). Arrows indicate the shift direction as RT increases. All spectra in each panel were run with t_{RcvyD} of 246 ms for R_1 and 250 ms for R_2, and with 3.3 kHz WALTZ-16 ^{15}N decoupling during t_2 acquisition, where applicable.

during data analysis. Moreover, changes in RF coil temperature in a relaxation series caused by a varying duty cycle will affect tuning and hence the reproducibility of the experiment.

The heating effects become worse for spectrometers operating at higher frequencies, where RF heating of sample (and coils) is more efficient. Hence, the application of relaxation experiments for larger proteins, which require higher field spectrometers for resolution and sensitivity, is particularly affected by these problems. The problem is further exacerbated when rapid recycling is required to economize on instrument time in high through-put applications.

We are not the first group to observe these problems and to suggest a solution. Setting very long recovery delays (τ_{RD}) [26,27] has been suggested, but such is clearly not the most efficient solution for the problem. Several ways of adding 'dummy' irradiation schemes [27–31] have been proposed, but these methods have as draw back that the recovery delay becomes variable, which is very undesirable. More elaborate schemes such as adjusting instrumental external temperature settings [30,32] per experiment or interleaving of not only the individual experiments but also scan by scan [32], have also been proposed.

In this paper, we propose a simple and robust scheme in which both total irradiation as well as the recycle delay remains constant throughout a relaxation series. This is achieved by combining a 'dummy' irradiation scheme which in our case is an *exact* copy of the relaxation block in all of its aspects, here called duty cycle compensation (DCC), with an efficient pre-scan ^{1}H saturation sequence (PSS). The proposed scheme keeps all spin-physics and instrumental parameters rigorously constant throughout the relaxation series. When combined with improvements that reduce the dependencies of the relaxation sequences on RF offset and pulse imperfections, relaxation experiments are obtained that can be used to identify subtle variations in relaxation rates, as is required for the determination of rotational diffusion anisotropy, CSA tensor determination, advanced motional modeling or entropy difference estimations. The methods are verified with ^{15}N spin relaxation experiments using human ubiquitin.

2. Materials and methods

2.1. Spectroscopy

All experiments were carried out with ^{15}N labeled human ubiquitin (20 mg/ml in a 90% H_2O/10% D_2O solution, pH 5.2, Spectra Stable Isotopes, Columbia, MD), using a Bruker Avance 500 MHz spectrometer at a nominal sample temperature of 298 K. All experiments were carried out using the pulse schemes described in Fig. 1 and in the results section.

The customary pulse schemes (called version 1 (v_1) without DCC and PSS, are shown in Fig. 1A), while with the proposed pulse schemes (v_2 with DCC and PSS) are shown for both ^{15}N T_1 and T_2-CPMG in Fig. 1B. The performance of these experiments was investigated. The total recovery delay (t_{RcvyD}) was varied with eight settings, covering a range of 0.2458 s (at 20 scans per t_1 point) to 1.5 s (at 4 scans per t_1 point) for T_1 experiments. For v_1 schemes t_{RcvyD} is equal to the data acquisition time (τ_{AQ}, 245.8 ms) plus the recovery delay (τ_{RD}), and for v_2 schemes t_{RcvyD} is equal to τ_{RD}.

Each relaxation-series (RS) consisted of three 2D experiments with RTs of 10, 170, and 740 ms for T_1 and 2.8, 33.6, and 98 ms for T_2-CPMG. All RSs were repeated in triplicate for statistic data analysis.

2.2. Data analysis

All spectra were processed with NMRPipe [33]. Peak picking and peak intensity quantification was carried out in NMRView [34]. Peak intensity magnitudes within each RS were collected and sorted by decay time (t in seconds) for rate analysis. Finally, rates (in s^{-1}) were calculated by least squares fitting to a single exponential of the form $I(t) = I(0)e^{-(t\cdot\mathrm{rate})}$.

We made the a priori assumption that the rates of the RSs are independent of the changes in the RS settings (among the same rate type T_1 or T_2), so that the average of the corresponding peak rates for the various triplicate RSs can be used to 'normalize' the relaxation rates of the various cross-peaks in the spectrum of ubiquitin to a standardized value. The remaining spread in the rates is a result of the precision of the RS experiments.

3. Results and discussion

The traditional (v_1) pulse scheme (Fig. 1A) leads to a relaxation-time (RT) dependent sample temperature change as shown in Figs. 2A, C, and G. For the v_1 T_1 experiment, in which few ^{1}H RF pulses are given during the RT, it is the ^{15}N acquisition decoupling that is the dominant cause of sample heating, as is demonstrated by turning it off (see Fig. 2E). When the decoupling is *on*, the overall RF duty-cycle decreases as the T_1 RT increases, leading to sample cooling when RT increases, which leads to the (apparent) up field peak shifts. Physically, the decoupling RF heats the ^{15}N RF coils. The amount of heat generated is dependent on the probe's RF efficiency. The heat of the coil is more or less efficiently transferred to the sample, depending cooling air flow (design). To avoid the heating, one may opt to reduce the ^{15}N decoupling power, but reduction in power may lead to incomplete decoupling with concomitant perturbation of the cross-peak lineshape and associated quantitation problems. The acquisition decoupling can be totally eliminated using TROSY detection [35], but this is not the most efficient detection scheme for small molecules and/or experiments at 600 MHz or less. As we will show below, decoupling is not the main source of heating in R_2-CPMG experiments; hence, TROSY detection to avoid decoupling heating can not be the generic solution.

Ultimately, it is desirable to induce a consistent amount of irradiation as uniformly distributed throughout the entirety of the relaxation experiment as possible. As others have shown before us, this can be achieved by introducing a duty cycle compensation (DCC) block of pulses and delays that compensate for the lack of pulses and delays found in the shortest RT experiment [27–30]. The DCC is a loop that more or less duplicates the RT loop scheme in the RT block with the number of loop repetitions for the DCC block adjusted such that the total time of DCC plus RT is constant for all spectra in the RS.

However, this solution by itself is worse than the problem: it will lead to a variation of the total recovery delay t_{RcvyD} which is given by τ_{AQ} (data acquisition time) + τ_{DCC} (total DCC time) + τ_{RD} (recovery delay), hence varying the input Z-magnetization H_z(in) over the RS, which is in this case given by

$$H_z(\mathrm{in}) = H_z(\mathrm{eq})\left(1 - e^{-(\tau_{\mathrm{AQ}}+\tau_{\mathrm{DCC}}+\tau_{\mathrm{RD}})/T_1^{\mathrm{H}}}\right), \qquad (1)$$

where H_z(eq) is the equilibrium magnetization and T_1^{H} is T_1 of the amide proton. In other words, in experiments with a shorter DCC (corresponding to those with the longest RT) H_z(in) is reduced, and vice-versa, leading to an artificially increased R_1 relaxation rate. Of course, this problem can be reduced by making τ_{RD} very long such that the change in DCC becomes irrelevant as suggested by [26]. Such may happen when $\tau_{\mathrm{RD}} \gg 3 * T_1^{\mathrm{H}}$ or minimally about 3 s.

To avoid this waste of instrument time, while retaining the benefits of the DCC block, we propose to implement after the DCC, but before the τ_{RD}, a pre-scan saturation block, or PSS block. The PSS block consists of a $\pi/2$ pulse on the ^{1}H nuclei followed by a field gradient pulse, finishing with a 1 ms high-power 'spin-lock' on the same nuclei again followed by a gradient pulse (see Fig. 1B). Control experiments with this sequence directly followed by data acquisition or followed by a $\pi/2$ pulse on the ^{1}H nuclei prior to data acquisition, showed that this sequence saturates all proton resonances so well that not even a residual water signal could be observed. Thus, the PSS sequence completely 'resets' the Z-magnetization to 'zero' irrespective of the state of the ^{1}H magnetization prior to it. Hence, the DCC block can be taken as an *exact* copy of the relaxation block, including pulse lengths, shapes, powers and offsets on all channels. This distinguishes our DCC block from DCC blocks in earlier proposals, where either the ^{1}H

pulses were omitted, or the ^{1}H carrier was changed [26]. After a constant τ_{RD} recovery period, the PSS thus enables a constant input ^{1}H Z-magnetization over the entire RS independent of the DCC time, as given by

$$H_z(\text{in}) = H_z(\text{eq})\left(1 - e^{-\tau_{RD}/T_1^H}\right). \quad (2)$$

With the implementation the DCC and PSS blocks as described in the legend of Fig. 1B, we observe for the T_1 experiment with ^{15}N-decoupling a significant improvement in temperature stability, as shown in Fig. 2B. The residual small peak position variations can be neglected for data analysis.

In contrast to the T_1 experiments, the T_2-CPMG experiments show very little change in the chemical shift whether ^{15}N acquisition decoupling is enabled (Fig. 2C) or not (Fig. 2G). This demonstrates that the T_2-CPMG RT loop scheme is the primary contributor to the sample heating. In this case, the overall RF duty-cycle increases as the T_2-CPMG RT increases, hence leading to sample heating and apparent downfield shifts, opposite to that of T_1. Inclusion of the DCC and PSS blocks (Figs. 2D and H) completely suppresses the artifact, demonstrating the efficacy of the new scheme in maintaining consistent duty cycle density and hence constant sample heating.

It may appear that τ_{RD} needs to be very long to achieve a sensitivity that is comparable to conventional NMR relaxation experiments. However, the differences are not large: in our experiment, the amount of "input" amide proton Z-magnetization, is given by Eq. (2). In the conventional experiment, formally the first 90° ^{1}H pulse of the reverse inept, of the sensitivity enhanced INEPT or of the TROSY block saturates all ^{1}H spin systems. Hence, the true magnetization recovery time in these experiments is given by

$$H_z(\text{in}) = H_z(\text{eq})\left(1 - e^{-(\tau_{RD}+\tau_{INEPT}+\tau_{AQ})/T_1^H}\right). \quad (3)$$

With the typical values $\tau_{RD} = 1$ s, $\tau_{INEPT} = 5.5$ ms, $\tau_{AQ} = 256$ ms, and $T_1^H = 1$ s, one obtains $H_z(\text{in}) = 0.63$ $H(\text{eq})$ for our scheme and H_z (in) $= 0.72$ $H(\text{eq})$ for the conventional experiment. The difference of 14% in favor of the conventional scheme is not dramatic.

For optimal recovery efficiency of 2D experiments, the value of τ_{RD} should be chosen such that the function

$$H_z(\text{in}) \propto \frac{1 - e^{-\tau_{RD}/T_1^H}}{\sqrt{\tau_{RD} + \tau_{EXP}}} \quad (4)$$

is at a maximum, where τ_{EXP} represents the time for a single pass through the pulse sequence not including τ_{RD}. Sample graphs for this equation, which takes into account the recovery of saturation (numerator) and signal averaging (denominator) are shown in Fig. 3.

To test the robustness of our method when using very short τ_{RD} settings, we measured relaxation series for various τ_{RD} settings. The data was analyzed and the rate

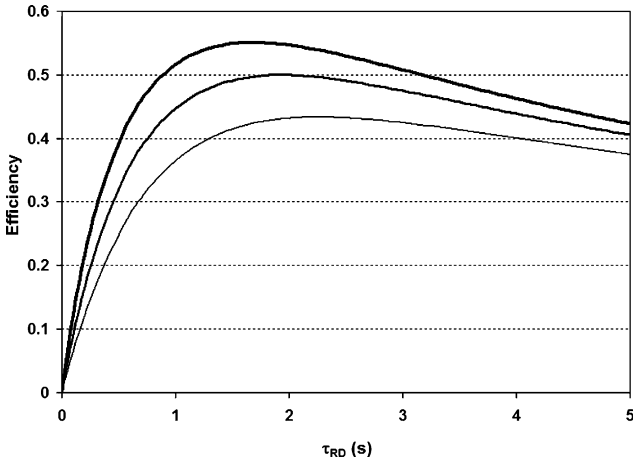

Fig. 3. Plot of the optimization function, $H_z(\text{in}) \propto \left\{1 - e^{-\left(\frac{\tau_{RD}}{T_1^H}\right)}\right\} / \sqrt{\tau_{RD} + \tau_{EXP}}$, where T_1^H was taken as 1 s, and τ_{EXP} as 0.5, 1, and 2 s for the thick, thinner and thin curves, respectively.

values for the different residues within each RS were standardized as described in methods. Fig. 4A depicts an unexpected, but significant trend in the v_1 T_1 experiment as a function of τ_{RD}: the apparent average R_1 decreases by 5% as τ_{RD} decreases. The artifact at short τ_{RD} can be attributed to a systematic underestimation of the intensities of the first few points of the RS when the RT is short: at these conditions much heating occurs, leading to changes in the spectrometer parameters (amplifier heating, RF coil heating), in turn affecting the tuning of the probe and amplifiers, leading to non-ideal RF pulses. For the larger decay points (740 ms RT) the duty cycle is less dense causing much less heating even for short values of τ_{RD}. Together this leads to an underestimation of the measured R_1 rate for small τ_{RD}. In the limit of large τ_{RD}, the 'true' R_1 rate is revealed.

Fig. 4B shows that the v_2 scheme with DCC and PSS, the obtained R_1 rate is independent of the setting of τ_{RD}, even at very short values of τ_{RD}. This is an important improvement, which can be exploited for relatively rapid acquisition of relaxation series when sensitivity is not limiting, such as on cryo-probe equipped spectrometers or concentrated solutions of small proteins in high-throughput applications.

It is possible to further improve the temperature stability within a single relaxation data point, by eliminating the variation in duty cycle when the indirect evolution period t_1 increases. This can be achieved by using constant time t_1 evolution (at a sensitivity cost), or, as suggested previously, by compensating for the changing t_1 by using a dummy cycle [31]. In our method, the latter can be implemented with a dummy time decrementing with t_1, prior to the PSS.

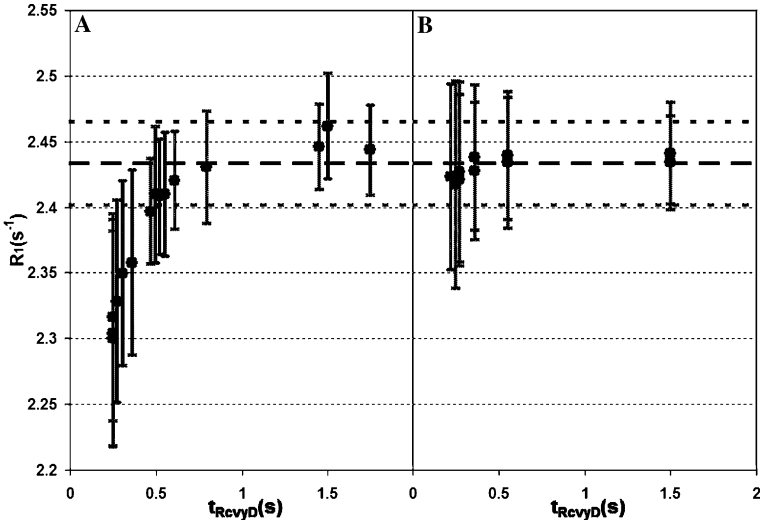

Fig. 4. The apparent 'global' average standardized ^{15}N R_1 relaxation rate for ubiquitin as a function of the total recovery delay t_{RcvyD} with ^{15}N acquisition decoupling enabled. (A) v_1 scheme without DCC or PSS, for t_{RcvyD} (s) $= \tau_{AQ} + \tau_{RD}$ ranging from 0.2458 to 1.7458 s; number of scans = 20, 16, 12, 8, or 4. (B) v_2 scheme with DCC and PSS, for t_{RcvyD} (s) $= \tau_{RD}$ ranging from 0.22, 0.24, 0.27, 0.36, 0.55, and 1.5 s; and number of scans = 20, 16, 16, 12, 8, and 4, respectively. The error bars represent ±1 standard deviation of the distribution of the resulting standardized peak rates in the corresponding RS.

Since the typical set of relaxation experiments consists of T_1, T_2, and NOEs, the ultimate aim is to provide consistent sample temperature throughout the entire set of different relaxation experiments. A manageable procedure is to adjust the external temperature settings for the different experiments such that sample temperature is consistent, as first suggested by [30,32]. This is implemented by comparing the ^1H chemical shifts in 1D test experiments of R_1, R_2, and NOE. Another approach might be to execute the entire set of relaxation experiments in scan by scan interleave mode [32], but this requires intensive experimental coding for spectrometer execution as well as untangling of the acquired data for processing.

Our method uses a complete saturation of all ^1H resonances, including solvent, to create a well-defined common "reset" point. As a consequence, the signal intensities of exchangeable NH resonances are reduced as compared to an experiment in which it is attempted to keep the solvent resonance at equilibrium. In principle, all ^1H pulses in the relaxation blocks and saturation pulses can be shaped such that the solvent resonance is not irradiated, with concomitant increase of sensitivity of the before mentioned resonances. However, we do no recommend such implementation for protein relaxation studies, since it is virtually impossible to create selective ^1H pulses that have a good amide proton excitation profile in the region 12–6 ppm, but which leave the solvent signal completely unperturbed, a prerequisite for the most accurate quantitative relaxation experiments. Good selective excitation without perturbing the solvent is however quite feasible for the nucleic acid imino proton range of 10–15 ppm. Thus, for imino nitrogen relaxation studies, we recommend the implementation of selective ^1H pulses to keep (return) the solvent resonance to equilibrium, for increased sensitivity.

4. Conclusion

The proposed duty cycle compensation with pre-scan saturation NMR spin-relaxation protocol significantly improves the performance of these experiments. The improvement can be demonstrated with respect to sample temperature stability and precision of data analysis, and more importantly, with respect to obtaining more accurate relaxation parameter values. The protocol can be applied to all types of NMR relaxation and relaxation dispersion experiments. These approaches can be combined with improvements that reduce the dependencies of the relaxation sequences on RF offset and pulse imperfections, to create relaxation experiments that can be used to identify subtle variations in relaxation rates, as is required for the determination of rotational diffusion anisotropy, CSA tensor determination, or advanced motional modeling and entropy difference estimations.

Acknowledgments

This work was supported by NIH GM 63027, NSF MCB 0135330 and by DOE 121415 sub-project "Experimental Elucidation of Molecular Machines". We thank Dr. Alexander V. Kurochkin for the maintenance of the NMR spectrometers, Dr. Tianzhi Wang for valuable

discussions, and the NIH, NSF and W.F. Keck foundation for funds towards the purchase of the NMR spectrometers used.

References

[1] G. Barbato, M. Ikura, L.E. Kay, R.W. Pastor, A. Bax, Backbone dynamics of calmodulin studied by ^{15}N relaxation using inverse detected two-dimensional NMR spectroscopy: the central helix is flexible, Biochemistry 31 (1992) 5269–5278.

[2] A.M. Mandel, M. Akke, A.G. Palmer, Backbone dynamics of *Escherichia coli* ribonuclease Hi—correlations with structure and function in an active enzyme, J. Mol. Biol. 246 (1995) 144–163.

[3] V.A. Feher, J. Cavanagh, Millisecond-timescale motions contribute to the function of the bacterial response regulator protein Spo0F, Nature 400 (1999) 289–293.

[4] A.L. Lee, A.J. Wand, Microscopic origins of entropy, heat capacity and the glass transition in proteins, Nature 411 (2001) 501–504.

[5] L. Maler, J. Blankenship, M. Rance, W.J. Chazin, Site-site communication in the EF-hand Ca^{2+}-binding protein calbindin D9k, Nat. Struct. Biol. 7 (2000) 245–250.

[6] L.C. Wang, Y.X. Pang, T. Holder, J.R. Brender, A.V. Kurochkin, E.R.P. Zuiderweg, Functional dynamics in the active site of the ribonuclease binase, Proc. Natl. Acad. Sci. USA 98 (2001) 7684–7689.

[7] S.Y. Stevens, S. Sanker, C. Kent, E.R.P. Zuiderweg, Delineation of the allosteric mechanism of a cytidylyltransferase exhibiting negative cooperativity, Nat. Struct. Biol. 8 (2001) 947–952.

[8] E.Z. Eisenmesser, D.A. Bosco, M. Akke, D. Kern, Enzyme dynamics during catalysis, Science 295 (2002) 1520–1523.

[9] L.E. Kay, D.A. Torchia, A. Bax, Backbone dynamics of proteins as studied by ^{15}N inverse detected heteronuclear NMR spectroscopy: application to staphylococcal nuclease, Biochemistry 28 (1989) 8972–8979.

[10] L. Zeng, M.W.F. Fischer, E.R.P. Zuiderweg, Study of protein dynamics in solution by measurement of C-13(alpha)-(CO)-C-13 NOE and (CO)-C-13 longitudinal relaxation, J. Biomol. NMR 7 (1996) 157–162.

[11] O. Millet, D.R. Muhandiram, N.R. Skrynnikov, L.E. Kay, Deuterium spin probes of side-chain dynamics in proteins. 1. Measurement of five relaxation rates per deuteron in (13)C-labeled and fractionally (2)H-enriched proteins in solution, J. Am. Chem. Soc. 124 (2002) 6439–6448.

[12] J.W. Peng, G. Wagner, Mapping of the spectral densities of N–H bond motions in eglin c using heteronuclear relaxation experiments, Biochemistry 31 (1992) 8571–8586.

[13] A.G. Palmer III, C.D. Kroenke, J.P. Loria, Nuclear magnetic resonance methods for quantifying microsecond-to-millisecond motions in biological macromolecules, Methods Enzymol. 339 (2001) 204–238.

[14] R. Bruschweiler, X. Liao, P.E. Wright, Long-range motional restrictions in a multidomain zinc-finger protein from anisotropic tumbling, Science 268 (1995) 886–889.

[15] N. Tjandra, D.S. Garrett, A.M. Gronenborn, A. Bax, G.M. Clore, Defining long range order in NMR structure determination from the dependence of heteronuclear relaxation times on rotational diffusion anisotropy, Nat. Struct Biol. 4 (1997) 443–449.

[16] D. Fushman, D. Cowburn, Nuclear magnetic resonance relaxation in determination of residue-specific ^{15}N chemical shift tensors in proteins in solution: protein dynamics, structure, and applications of transverse relaxation optimized spectroscopy, Methods Enzymol. 339 (2001) 109–126.

[17] D. Fushman, N. Tjandra, D. Cowburn, Direct measurement of ^{15}N chemical shift anisotropy in solution, J. Am. Chem. Soc. 120 (1998) 10947–10952.

[18] N. Tjandra, A. Szabo, A. Bax, Protein backbone dynamics and ^{15}N chemical shift anisotropy from quantitative measurement of relaxation interference effects, J. Am. Chem. Soc. 118 (1996) 6986–6991.

[19] R. Bruschweiler, M. Blackledge, R.R. Ernst, Multi-conformational peptide dynamics derived from NMR data: a new search algorithm and its application to antamanide, J. Biomol. NMR 1 (1991) 3–11.

[20] M.W.F. Fischer, L. Zeng, Y.X. Pang, W.D. Hu, A. Majumdar, E.R.P. Zuiderweg, Experimental characterization of models for backbone picosecond dynamics in proteins. Quantification of NMR auto- and cross-correlation relaxation mechanisms involving different nuclei of the peptide plane, J. Am. Chem. Soc. 119 (1997) 12629–12642.

[21] M.W. Fischer, L. Zeng, A. Majumdar, E.R. Zuiderweg, Characterizing semilocal motions in proteins by NMR relaxation studies, Proc. Natl. Acad. Sci. USA 95 (1998) 8016–8019.

[22] D. Bytchenkoff, P. Pelupessy, G. Bodenhausen, Anisotropic local motions and location of amide protons in proteins, J. Am. Chem. Soc. 127 (2005) 5180–5185.

[23] M. Akke, R. Bruschweiler, A.G. Palmer, NMR order parameters and free-energy—an analytical approach and its application to cooperative Ca^{2+} binding by calbindin-D(9k), J. Am. Chem. Soc. 115 (1993) 9832–9833.

[24] D. Yang, Y.K. Mok, J.D. Forman-Kay, N.A. Farrow, L.E. Kay, Contributions to protein entropy and heat capacity from bond vector motions measured by NMR spin relaxation, J. Mol. Biol. 272 (1997) 790–804.

[25] A.L. Lee, S.A. Kinnear, A.J. Wand, Redistribution and loss of side chain entropy upon formation of a calmodulin–peptide complex, Nat. Struct Biol. 7 (2000) 72–77.

[26] S.M. Gagne, S. Tsuda, L. Spyracopoulos, L.E. Kay, B.D. Sykes, Backbone and methyl dynamics of the regulatory domain of troponin C: anisotropic rotational diffusion and contribution of conformational entropy to calcium affinity, J. Mol. Biol. 278 (1998) 667–686.

[27] G. Lippens, J.M. Wieruszeski, D. Horvath, P. Talaga, J.P. Bohin, Slow dynamics of the cyclic osmoregulated periplasmic glucan of *Ralstonia solanacearum* as revealed by heteronuclear relaxation studies, J. Am. Chem. Soc. 120 (1998) 170–177.

[28] F.A.A. Mulder, P.J.A. van Tilborg, R. Kaptein, R. Boelens, Microsecond time scale dynamics in the RXR DNA-binding domain from a combination of spin–echo and off-resonance rotating frame relaxation measurements, J. Biomol. NMR 13 (1999) 275–288.

[29] Y. Hashimoto, S.P. Smith, A.R. Pickford, A.A. Bocquier, I.D. Campbell, J.M. Werner, The relative orientation of the fibronectin 6F1(1)F2 module pair: a ^{15}N NMR relaxation study, J. Biomol. NMR 17 (2000) 203–214.

[30] J.M. Werner, V. Knott, P.A. Handford, I.D. Campbell, A.K. Downing, Backbone dynamics of a cbEGF domain pair in the presence of calcium, J. Mol. Biol. 296 (2000) 1065–1078.

[31] A.C. Wang, A. Bax, Minimizing the effects of radiofrequency heating in multidimensional NMR experiments, J. Biomol. NMR 3 (1993) 715–720.

[32] D.M. Korzhnev, M. Billeter, A.S. Arseniev, V.Y. Orekhov, NMR studies of Brownian tumbling and internal motions in proteins, Prog. Nucl. Magn. Reson. Spectros. 38 (2001) 197–266.

[33] F. Delaglio, S. Grzesiek, G.W. Vuister, G. Zhu, J. Pfeifer, A. Bax, NMRPipe—a multidimensional spectral processing system based on unix pipes, J. Biomol. NMR 6 (1995) 277–293.

[34] B.A. Johnson, R.A. Blevins, NMR view—a computer-program for the visualization and analysis of NMR data, J. Biomol. NMR 4 (1994) 603–614.

[35] G. Zhu, Y. Xia, L.K. Nicholson, K.H. Sze, Protein dynamics measurements by TROSY-based NMR experiments, J. Magn. Reson. 143 (2000) 423–426.

[36] G.N. Yip, E.R. Zuiderweg, A phase cycle scheme that significantly suppresses offset-dependent artifacts in the *R*(2)-CPMG ^{15}N relaxation experiment, J. Magn. Reson. 171 (2004) 25–36.

[37] A.J. Shaka, J. Keeler, T. Frenkiel, R. Freeman, An improved sequence for broadband decoupling: WALTZ-16, J. Magn. Reson. 52 (1983) 335–338.